SECOND EUROPEAN ROTORCRAFT AND POWERED
LIFT AIRCRAFT FORUM

Paper No. 13

ROTOR ISOLATION OF THE HINGELESS ROTOR BO-105 AND YUH-61 HELICOPTERS

R.A. Desjardins
and
W.E. Hooper

The Boeing Vertol Company
Philadelphia, Pennsylvania 19142

September 20 - 22, 1976

Buckeburg, Federal Republic of Germany

Deutsche Gesellschaft fur Luft- und Raumfahnt e.V.

Postfach 510645, D-5000 Koln, Germany

ROTOR ISOLATION OF THE HINGELESS ROTOR BO-105 AND YUH-61A HELICOPTERS

Rene A. Desjardins
Manager, Rotor Head, Controls and Vibration Design

W. Euan Hooper
Director of Technology
The Boeing Vertol Company

Abstract

This paper presents the development of an improved rotor isolation system (IRIS) applied to hingeless rotors to minimize helicopter vibrations. It describes specific design features required to achieve an exceptionally high degree of isolation in a compact environment where severe restrictions are placed on size, weight and range of available motion. The analysis, bench tests and full scale flight tests show a significant reduction of N/REV as well as 2N/REV vibration with no interference to the agility and handling qualities of the aircraft.

Notation

F	Rotor Excitation Force
K_1	Isolator Spring
K_3	Bar Spring for 2nd Frequency
l	Distance Transmission pivot to M_3
M_1	Transmission Rotor Equivalent Mass
M_2	Airframe Equivalent Mass
M_3	Bar Mass for 2nd Antiresonant Frequency
M_B	Bar Mass for 1st Antiresonant Frequency
r	Distance Xmsn Pivot to Airframe Pivot
R	Distance Transmission Pivot to M_B
TR	Transmissibility
Z_1	Rotor Mass Displacement
Z_2	Airframe Mass Displacement
Z_3	2nd Antiresonant Mass Displacement
ω	Frequency
ω_A	Antiresonant Frequency

Introduction

An increasing demand for the reduction of helicopter vibration has been dictated by the expansion of flight envelopes coupled with more stringent requirements for crew and passengers' comfort as well as improved reliability and maintainability. Today's helicopters are flying faster, new requirements limit vibration levels to ±0.05g, and Reliability and Maintainability characteristics, which are a function of vibration loads as reported in Reference 1, are receiving more attention in the design and evaluation of helicopters.

It is known that objectionable helicopter vibration is rotor induced. Experience has shown that fixed-system N/REV rotor vibratory loads, where N is an integer multiple of the blades per rotor, are the greatest contributors to helicopter fuselage vibration.

Different methods for reducing rotor induced fuselage vibration have, in the past, been considered. Structural dynamic tuning to control fuselage mode shape has been presented in Reference 2. Problems associated with this approach are primarily the variation of the shape of in-flight modes with fuselage loading and also higher vibration in areas of the fuselage far from the node points. Frahm type mass-spring, fixed tuned or self-tuning vibration absorbers, have been flown as reported in Reference 3. These absorbers were effective only in the vicinity of their location in the fuselage. Pendulum dynamic absorbers mounted in the rotating system (References 4, 5) have been effective in reducing of fuselage vibration but resulted in loss of aircraft performance due to drag penalty.

More recently, several approaches featuring rotor isolation have been successful and trends seem to indicate that rotor isolation is the solution to vibration problems.

A number of new isolation systems have been proposed or flown. The most simple approach is the conventional isolation; however, this solution is applicable only where rotor loads are relatively low. Conventional rotor isolation, applied to advanced rotors such as hingeless or bearingless rotors, would result in intolerable large deflections. Fully active devices or passive devices with active trim have been reported in References 6, 7 and 8. The advantage of these systems is a broad band isolation capability but at the expense of control and power to drive at the proper amplitude and phase. An attractive solution is the passive nodal isolation. Extensive work has been done in this area, mainly by the Kaman Corporation (Reference 9 and 10) and the Bell Company (Reference 11).

The purpose of this paper is to present the Boeing Vertol program to develop an effective, multi-axis, single and multi frequency nodal isolation system applied to hingeless rotor helicopters.

This Improved Rotor Isolation System (IRIS) has been designed fabricated, bench and flight evaluated on the BO-105 (Figure 1) and on the YUH-61A UTTAS (Figure 2) helicopters.

The prime objective of the program has been to demonstrate that a cockpit vibration level below 0.05g can be achieved on the YUH-61A. This was achieved first on the small and dynamically similar BO-105. The paper describes the evolution of the program from concept to flight test for both aircraft.

Figure 1. MBB BO-105 Helicopter

Figure 2. Boeing Vertol YUH-61A Helicopter

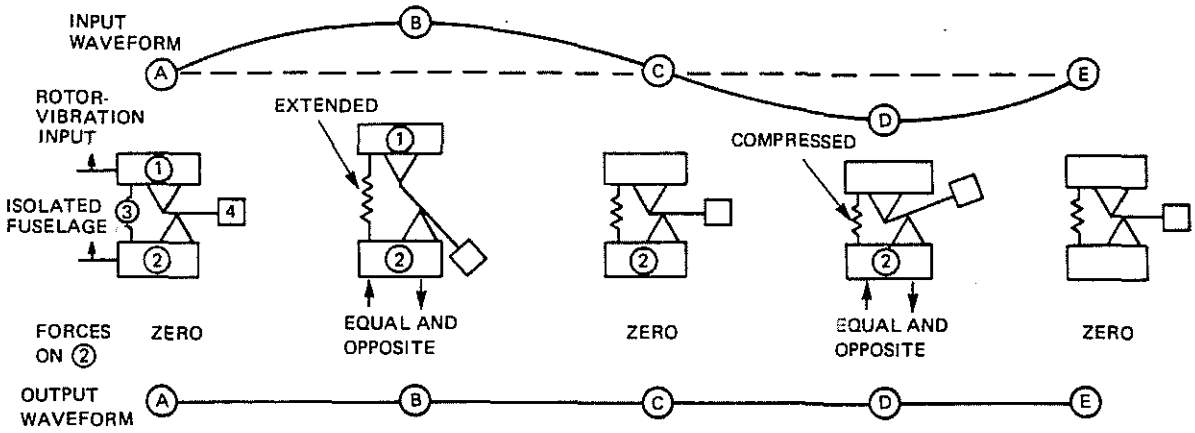

Figure 3. Concept of Rotor Isolation

Isolation Concept

The IRIS is a multi-axis rotor isolation system developed for hingeless rotors using the concept of nodalization already demonstrated by Kaman with the Davi[9, 10], and Bell with the nodamatic[11] for teetering rotors. The concept uses a combination of opposing spring and inertia forces to create a node, or point of zero vibration motion, at the airframe-attachment point, as shown in Figure 3.

Operation of the isolator can be followed in Figure 3. At A, the rotor-vibration input is at its neutral position, so the rotor 1, fuselage 2, spring 3, and antiresonant bar weight 4, are all at neutral. At B, rotor vibration is upward, so the rotor 1 moves up, the spring 3 is stretched, the bar weight 4 is moved downward, but the fuselage remains stationary. At C, the rotor vibration is returning through neutral, so all parts are neutral and fuselage vibration is still zero. At D, rotor vibration 1 is downward, the spring 3 is compressed, the bar weight 4 is moved upward, but the fuselage 2 is still zero. Finally E, is neutral like A, starting a new cycle.

The action of a nodal isolator differs significantly from a conventional isolator. A transmissibility plot for a conventional isolator has a resonant frequency and then isolates above a frequency ratio of $> \sqrt{2}$ with the isolation improving as the frequency increases, reaching 100-percent isolation at infinite frequency. A nodal isolator has a similar resonant frequency but then has a specific antiresonant frequency at which 100-percent isolation is achieved.

The isolation of a conventional isolator changes as the suspended gross weight changes. However, the nodal isolator achieves 100-percent isolation without regard to change in weight conditions. Furthermore, the spring rate used can be very stiff compared to the spring of a conventional isolator.

The ratio of airframe-mass motion to rotor-mass motion is referred to as transmissibility. When the transmissibility is plotted versus the frequency ratio of the applied force, and assuming no damping it is seen in Figure 4 that at the so-called antiresonant frequency the airframe mass has 100-percent isolation from the vibratory force.

The transmissibility in the region of the antiresonant frequency (referred to as the bucket) determines the rpm sensitivity that will be felt in the airframe. A measure of this rpm sensitivity is the width of the bucket at a transmissibility of 0.1. A simple analytical model of the YUH-61A isolator shows the width of the bucket at 23 percent, (Figure 5) which implies a wide range of rotor rpm over which satisfactory isolation will take place.

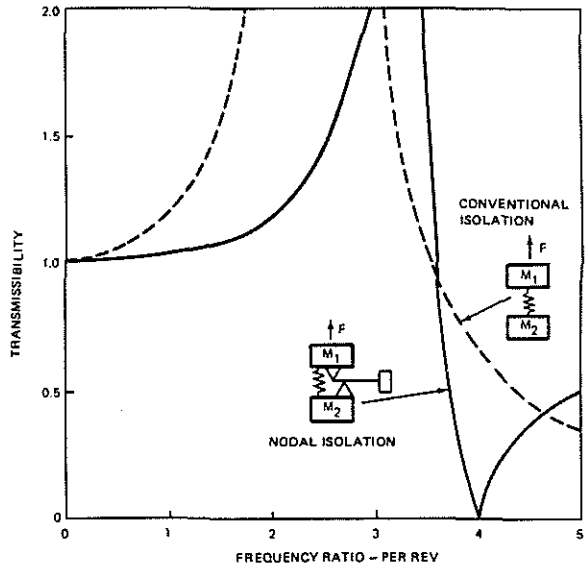

Figure 4. Comparison of Transmissibility

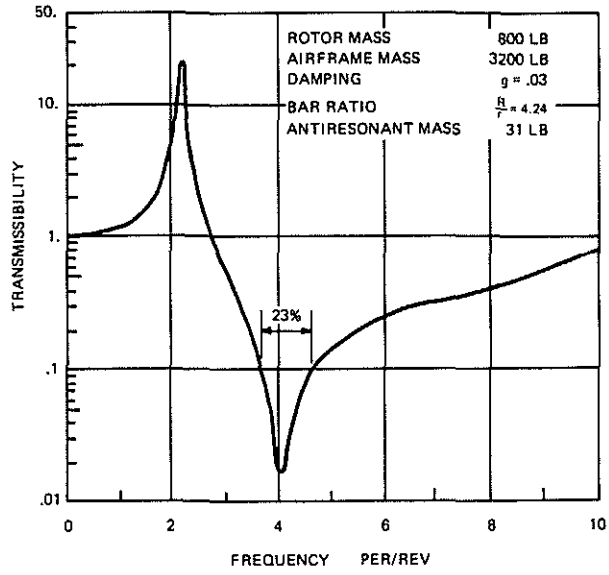

Figure 5. Analytical Transmissibility of Antiresonant Isolator

Analysis of the Improved Rotor-Isolation System

The analytical model of a single-frequency antiresonance isolator is shown in Figure 6. The equations of motion for masses M_1 (transmission) and M_2 (fuselage) are:

$$[M_1 + M_B(\frac{R}{r} - 1)^2]\ddot{Z}_1 - [M_B(\frac{R}{r} - 1)\frac{R}{r}]\ddot{Z}_2 + K(Z_1 - Z_2) = F_1 \sin \omega t$$

$$[M_B(\frac{R}{r} - 1)\frac{R}{r}]\ddot{Z}_1 + [M_2 + M_B(\frac{R}{r})]\ddot{Z}_2 + K(Z_2 - Z_1) = 0$$

If we choose the parameters M_B, r, R, and K such that at a predetermined frequency,

$$K - \omega_A^2 M_B(\frac{R}{r} - 1)\frac{R}{r} = 0,$$

the equations of motion become uncoupled (at $\omega = \omega_A$) and Z_2 the motion of M_2 (fuselage) goes to zero (at $\omega = \omega_A$) no matter what the values of F_1, Z_1, M_1 and M_2 are.

This isolation is achieved at $\omega = \omega_A$ by balancing the forces such that the inertial force exerted at pivot B by mass M_B on M_2 is exactly equal in magnitude, but opposite in direction to the spring force exerted by spring K on M_2. Thus, at $\omega = \omega_A$, the resultant forces acting on M_2 (fuselage) are zero, and thus the motion of M_2 is also zero.

Transmissibility, defined here as the ratio of airframe motion (Z_2) to transmission motion (Z_1), is:

$$TR = \frac{K - \omega^2[M_B(\frac{R}{r} - 1)\frac{R}{r}]}{K - \omega^2[M_2 + M_B(\frac{R}{r})^2]}$$

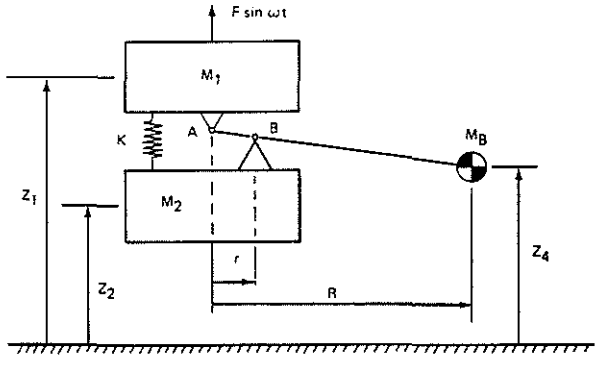

Figure 6. Mathematical Model of the Isolator

BO-105 Vibration Treatment

A program of vibration-device development suitable for the hingeless rotor has been in progress since 1972. The basic BO-105 with a 28-Hz, 4/REV vibration is acceptable above transition and to its 120-knot maximum speed. However, at transition speeds and in normal-approach descent and flare, vibration has been somewhat objectionable.

Initially, we developed a flap and lag pendulum absorber and blade-detuning weight to achieve an improved level. This resulted in significant reductions in level flight, transition, descent, and approach-flare vibration. Although these reductions were large, levels were still not down to a 0.05g goal.

The next program toward the goal was the first isolation system for the hingeless rotor. Working with Kaman Corporation, developers of the DAVI, an elastomeric-spring DAVI isolator was designed and built. The transmission was supported on an intervening H-frame (Figure 7) and the isolators placed at each corner, attaching to the airframe. The units (shown in Figure 8) were installed in the aircraft and a ground-shake test was conducted. Isolation was poor due to the damping of the elastomer and, in addition, the fatigue life of the spring was unacceptably low due to high stresses in the elastomer bond. This configuration was not flown.

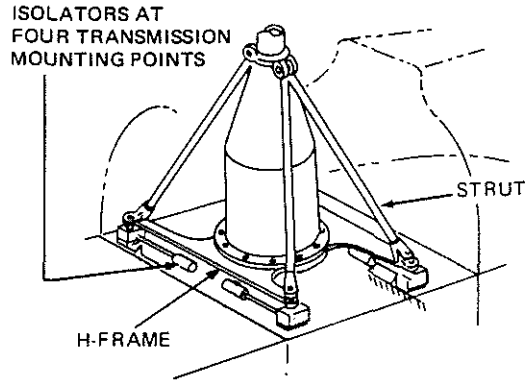

Figure 7. BO-105 Isolation System Installation

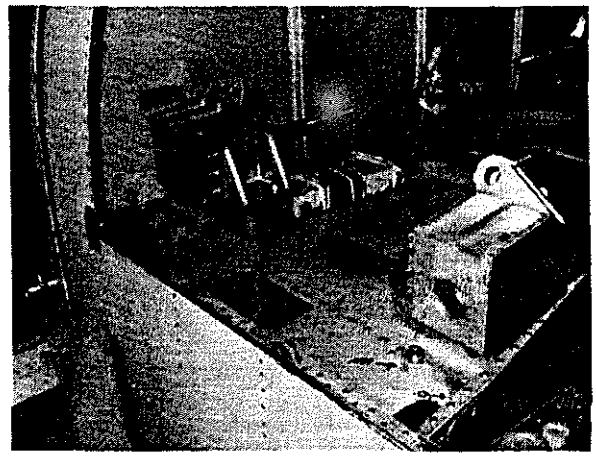

Figure 8. Elastomeric Isolator Unit Installed in the BO-105

A new program featuring metal spring isolator was then initiated in May 1975. Again, the rotor transmission was on an H-frame with a vertical isolator in each corner. This system gave isolation between the rotor transmission and the airframe in the pitch, roll, and vertical directions. The isolator, Figure 9, used a flexbeam vertical spring and a pivoted bar. Controls were redesigned to provide geometry that is not affected by deflections across the isolators. Engine-shaft couplings were changed to accommodate the relative motion.

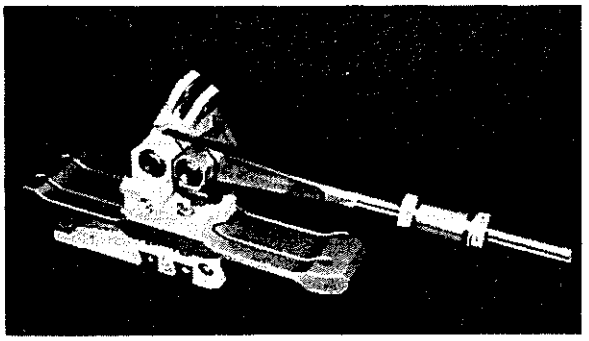

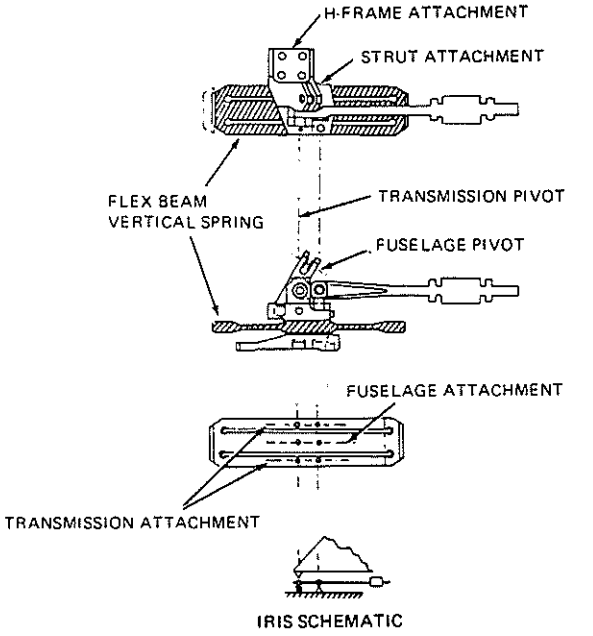

Figure 9. BO-105 Metal Isolator Unit

A tuning rig shown in Figure 10 was built and the metal isolator gave a transmissibility of 0.03 (97-percent isolation) as seen in Figure 11. The width of the bucket at a transmissibility of 0.1 is 11.7%. This was much improved over the elastomeric-isolation unit which had a transmissibility of 0.25 (75-percent isolation).

Flight-test results for this system were good in the vertical direction, as shown in Figure 12.

In the lateral direction, levels were not reduced confirming that lateral isolation was needed. The approach taken was the addition of a fifth antiresonant bar between the transmission and fuselage, acting in the lateral direction.

Level-flight results were now much improved and lateral vibration was reduced to below 0.1g, as shown in Figure 13.

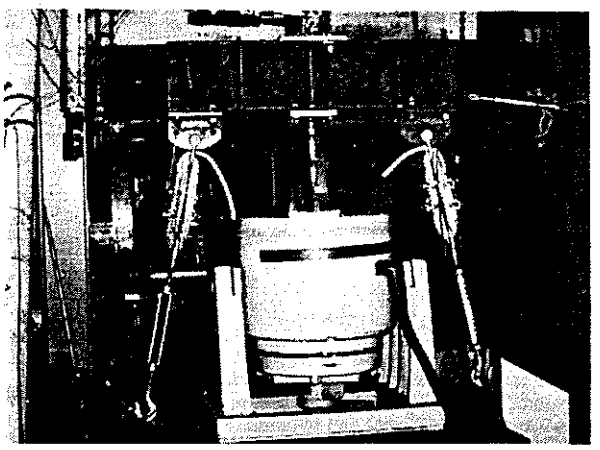

Figure 10. BO-105 Isolator Test Rig

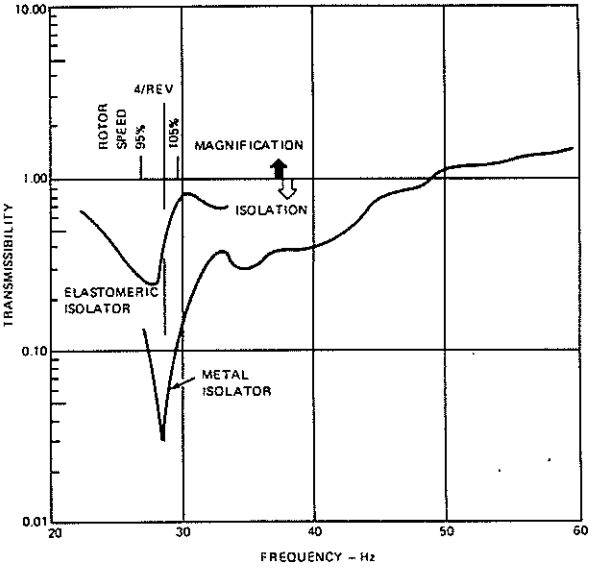

Figure 11. Comparison of Elastomeric & Metal Vibration Isolators in Bench Test

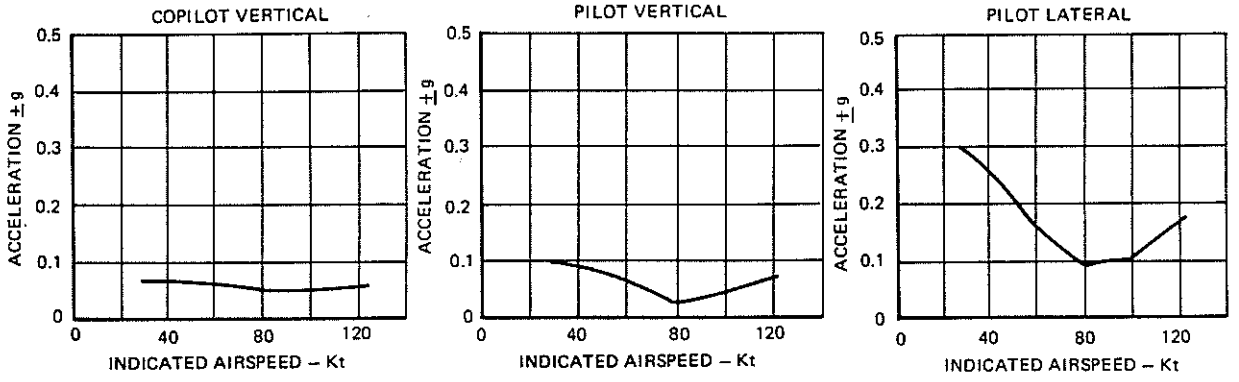

Figure 12. BO-105 In-Flight Vibration with Vertical Isolation

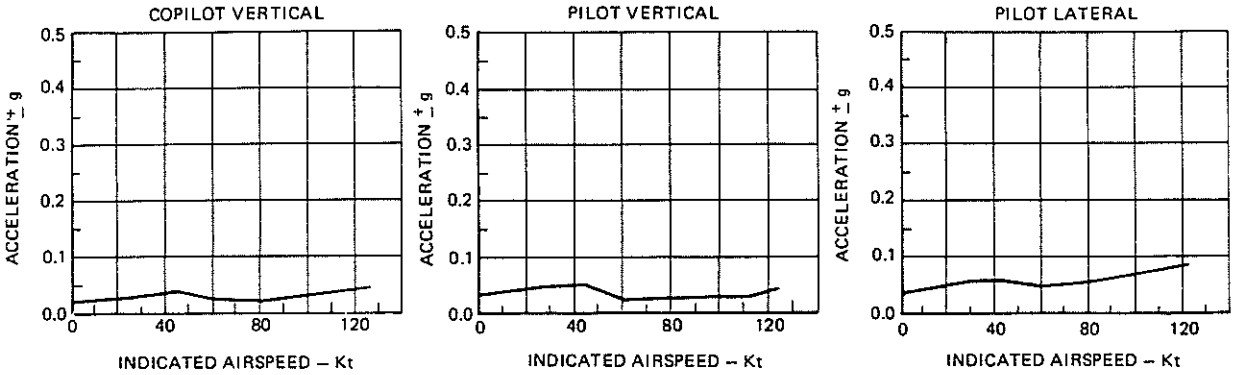

Figure 13. BO-105 In-Flight Vibration with Lateral Isolator Added to Vertical Isolator

Partial-power descent levels were also substantially improved for the 500-fpm 20 knot partial power descent, which provides the highest vibration for untreated BO-105. Figure 14 demonstrates the isolator low transmissibility over a large RPM variation resulting in cockpit levels shown in Figure 15.

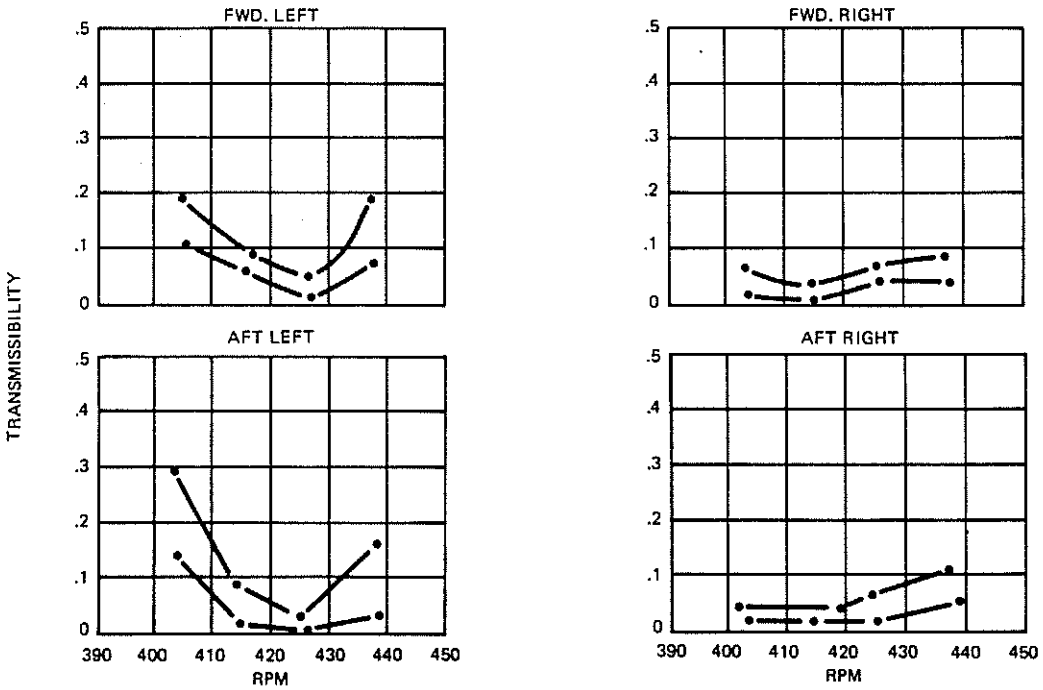

Figure 14. BO-105 In-Flight Metal Isolator Transmissibility

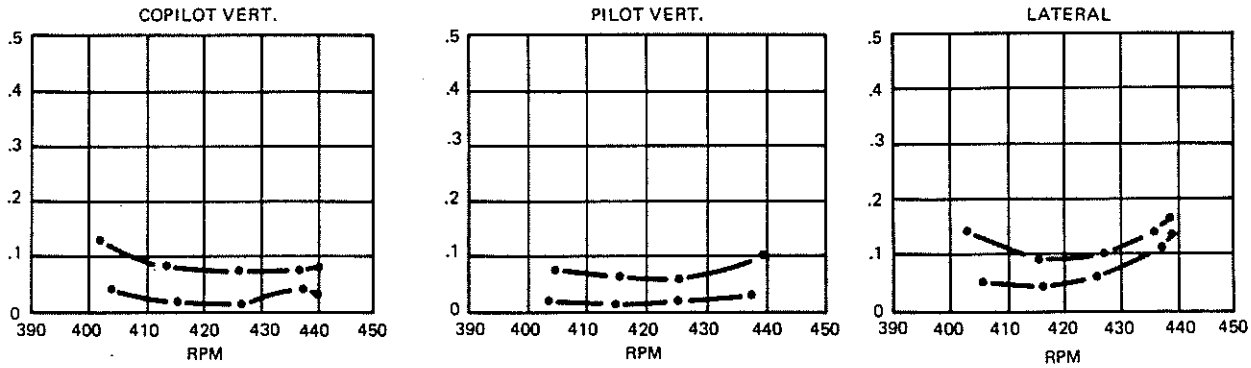

Figure 15. BO-105 RPM Sweep. Partial Power Descent 4Ω Vibration in Cockpit

Vibration in the normal approach and flare was much reduced, as seen in time history, Figure 16. The 4/REV vibration was reduced below the level of the residual 8/REV which is seen as the dark portion of the time history.

The behavior of the isolation during severe maneuvers is important. As shown in Figure 17, 2g banked turns produce no significant change in vibration and the same is true for a wide range of maneuvers from 0-2.5g. During the development testing of the IRIS bottoming was encountered at low g levels when, in error, the spring travels were approximately 60% of the design values.

The result of this was an immediate increase in vibration whenever bottoming occurred to levels somewhat lower than that of the original unisolated aircraft. An example of this is seen in Figure 18 during which successive 2g pullups and 0.5g pushovers first hit the stops and on the next pullup just did not hit the stops.

In summary, when bottoming was encountered its effect was no worse than to revert to the basic aircraft. However, in the final configuration the spring travel was sufficient to avoid bottoming for maneuvers well in excess of 2g.

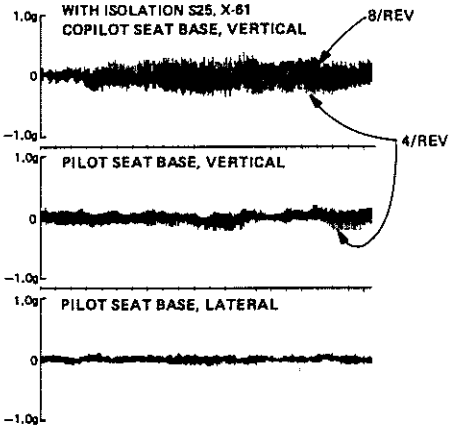

Figure 16. Time History – Peak 4/REV Vibration in Normal Approach BO-105

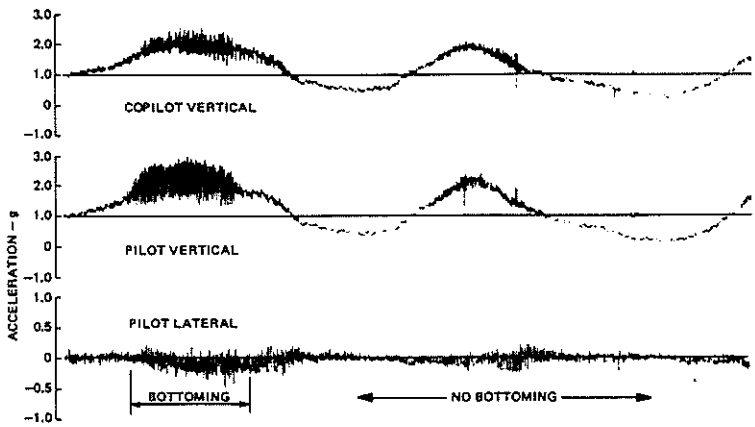

Figure 18. Effect on Cockpit Vibration of Isolation Bottoming

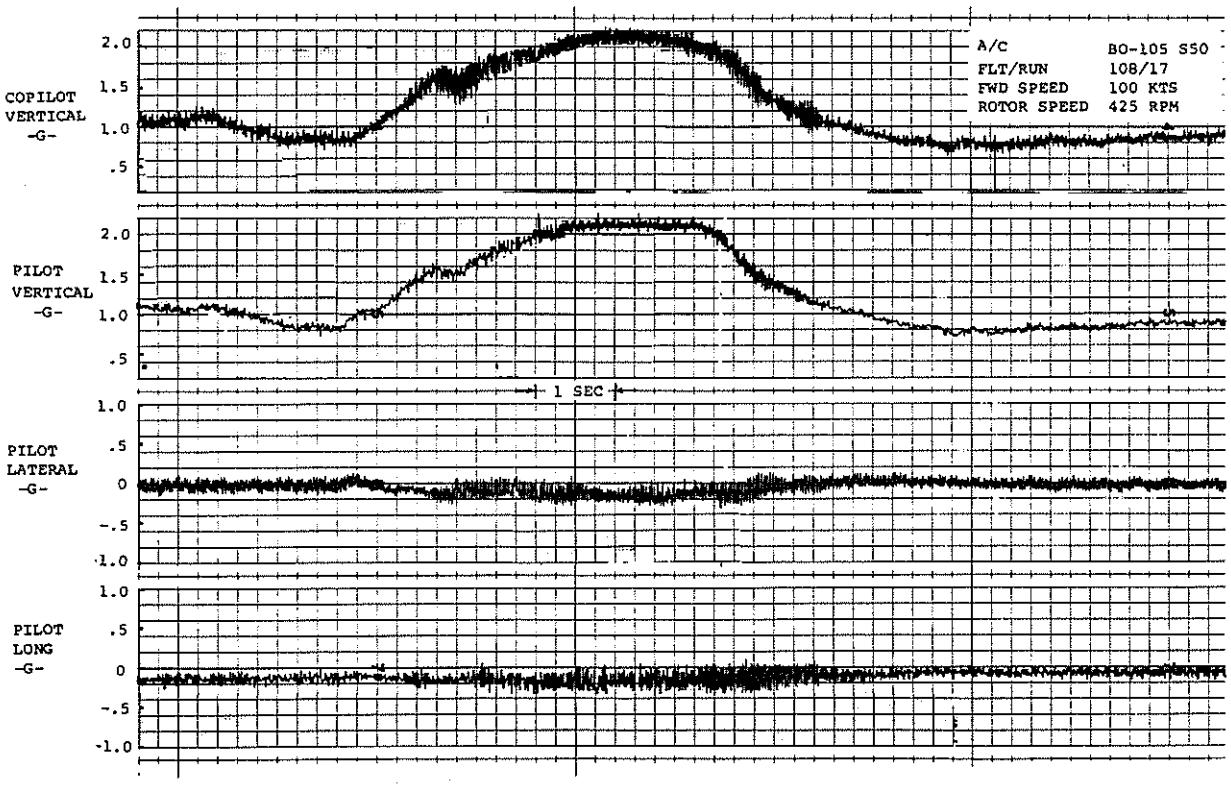

Figure 17. Cockpit vibration During A 60° Banked Turn

Multi-Frequency Isolator

With 4/REV vibration now very low, the residual 8/REV vibration is the 20 knot speed regime emerged as the vibration to which the pilots were most sensitive. This resulted in a simple but significant extension of the system to isolate 8/REV vibration in addition to the basic 4/REV. An innovative improvement to the basic isolator was incorporated in the BO-105 units which, with no compromise of effectivity in 4/REV isolation, substantially reduced 8/REV as a source of crew discomfort. In order to provide additional isolation at a second frequency, the bar is modified to be near resonance at 8/REV. The analytical model of the multi-frequency antiresonant isolator is shown in Figure 19. A spring mass is added to mass M_B such that a second frequency is introduced at which M_1 and M_2 becomes uncoupled.

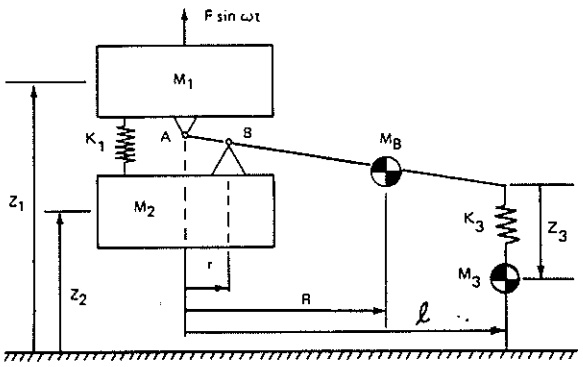

Figure 19. Multi-Frequency Isolator Analytical Model

The new equations of motion are:

$$[M_1 + M_B (\frac{R}{r} - 1)^2 + M_3 (\frac{\ell}{r})^2] \ddot{Z}_1$$

$$-[M_B (\frac{R}{r} - 1) \frac{R}{r} + M_3 (\frac{\ell}{r} - 1) \frac{1}{r}] \ddot{Z}_2$$

$$+ M_3 (\frac{\ell}{r} - 1) \ddot{Z}_3 + K_1 (Z_1 - Z_2) = F \sin \omega t$$

$$- [M_B (\frac{R}{r} - 1) \frac{R}{r} + M_3 (\frac{\ell}{r} - 1) \frac{\ell}{r}] \ddot{Z}_1$$

$$+ [M_2 + M_B (\frac{R}{r})^2 + M_3 (\frac{\ell}{r})^2] \ddot{Z}_2$$

$$- M_3 \frac{1}{r} \ddot{Z} + K_1 (-Z_1 + Z_2) = 0$$

$$M_3 (\frac{\ell}{r} - 1) \ddot{Z}_1 - M_3 \frac{\ell}{r} \ddot{Z}_2 + M_3 \ddot{Z}_3 + K_3 Z_3 = 0$$

or, in matrix form,

$$\begin{bmatrix} K_1 - \omega^2 M_{11} & -(K_1 - \omega^2 M_{12}) & -\omega^2 M_{13} \\ -(K_1 - \omega^2 M_{21}) & K_1 - \omega^2 M_{22} & \omega^2 M_{23} \\ -\omega^2 M_{31} & \omega^2 M_{32} & K_3 - \omega^2 M_{33} \end{bmatrix} \begin{Bmatrix} Z_1 \\ Z_2 \\ Z_3 \end{Bmatrix} = \begin{Bmatrix} F \\ 0 \\ 0 \end{Bmatrix}$$

where

$$M_{11} = M_1 + M_B (\frac{R}{r} - 1)^2 + M_3 (\frac{\ell}{r})^2$$

$$M_{12} = M_{21} = M_B (\frac{R}{r} - 1) \frac{R}{r} + M_3 (\frac{\ell}{r} - 1) \frac{\ell}{r}$$

$$M_{13} = M_{31} = M_3 (\frac{\ell}{r} - 1)$$

$$M_{22} = M_2 + M_B (\frac{R}{r})^2 + M_3 (\frac{\ell}{r})^2$$

$$M_{23} = M_{32} = M_3 \frac{\ell}{r}$$

$$M_{33} = M_3.$$

The solution for Z_2 can be formally written,

$$Z_2 = \frac{\begin{bmatrix} K_1 - \omega^2 M_{11} & F & -\omega^2 M_{13} \\ -(K_1 - \omega^2 M_{21}) & 0 & \omega^2 M_{23} \\ -\omega^2 M_{31} & 0 & K_3 - \omega^2 M_{33} \end{bmatrix}}{\Delta}$$

where Δ = determinant of dynamic matrix

The necessary and sufficient condition for Z_2 to become zero ($\Delta \neq 0$ at same time) is:

$$\begin{vmatrix} -(K_1 - \omega^2 M_{21}) & \omega^2 M_{23} \\ -\omega^2 M_{31} & K_3 - \omega^2 M_{33} \end{vmatrix} = 0,$$

which yields:

$$\omega^4 (M_{33} M_{12} - M_{31} M_{23}) - \omega^2 (K_1 M_{33} + K_3 M_{21}) + K_1 K_3 = 0$$

or, after some reduction,

$$M_3 M_B (\frac{R}{r} - 1) \frac{R}{r} \omega^4 - [K_1 M_3 + K_3 [M_3 (\frac{R}{r} - 1) \frac{R}{r} + M_3 (\frac{\ell}{r} - 1) \frac{\ell}{r}] \omega^2 + K_1 K_3 = 0.$$

Since this governing equation is a quadratic in ω^2, it is apparent that, with the proper choices of the variable parameters (K_1, K_3, M_B, R, r, ℓ), there should be two frequencies at which the desired goal of obtaining $Z_2 = 0$ can be achieved.

It turns out that isolation performance is virtually independent of the value of M_3 (as long as K_3 is changed accordingly) and that isolation characteristics are primarily dependent on the value of $\bar{I}_B$:

$$\bar{I}_B = M_B (R - r) R,$$

for it is predominantly this parameter which controls the resonant frequency between the 4/REV and 8/REV isolation frequencies. Increasing values of $\bar{I}_B$ broaden the isolation-frequency band near 4/REV because the resonant frequency (above 4/REV) is pushed upward closer to 8/REV.

The expression for transmissibility is easily obtained from the equations above:

$$TR = \frac{Z_2}{Z_1} = \frac{(K_1 - \omega^2 M_{21})(K_3 - \omega^2 M_{33}) - \omega^4 M_{31} M_3}{(K_1 - \omega^2 M_{22})(K_3 - \omega^2 M_{33}) - \omega^4 M_{23}^2}$$

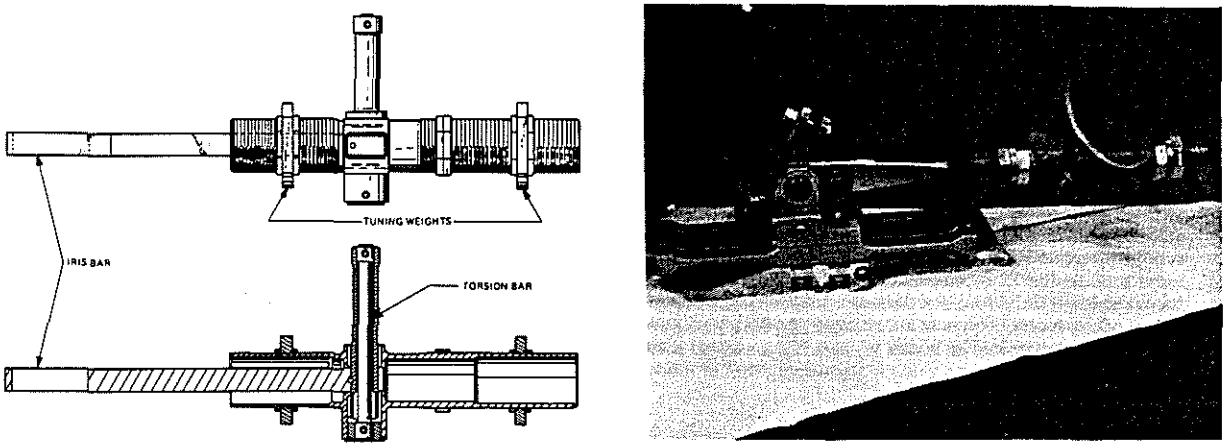

Figure 20. Dual Frequency Isolator Dwg and Installation

There will be two frequencies at which TR = 0 and two resonances, since both the numerator and denominator are second-order polynominals in ω^2.

Figure 20 shows the multi frequency isolator. An additional pivot axis is introduced along the antiresonant bar and a short torsion bar allows the outer portion of the antiresonant bar to be separately tuned. Movable weights on the outer portion primarily tune 4/REV when moved in the same direction and 8/REV when moved in opposite directions.

Bench tuning results show (Figure 21) the 4/REV bucket unchanged from the earlier single tuned unit. The width of the bucket at 0.1 transmissibility is unchanged at 12%. The 8/REV bucket gives better than 10-to-1 attenuation with extremely low rpm sensitivity.

Subsequent flight testing confirmed isolators low transmissibility as shown in Figure 22 resulting in cockpit levels below 0.1 g at 8/REV at normal rotor speed. Levels at 4/REV remained the same as they were with the single frequency isolator.

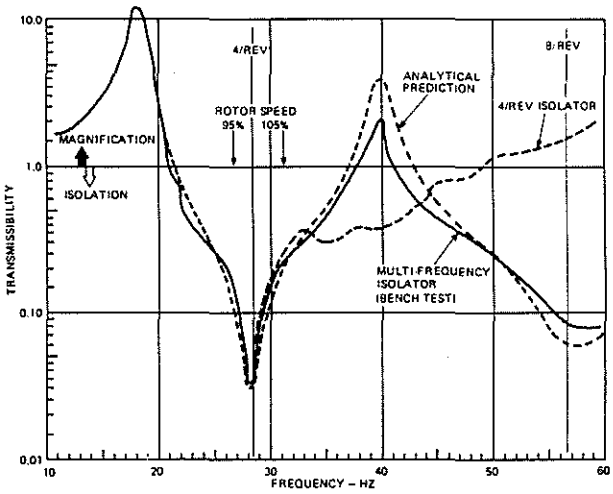

Figure 21. BO-105 Multi Frequency Isolator Analysis and Bench Test

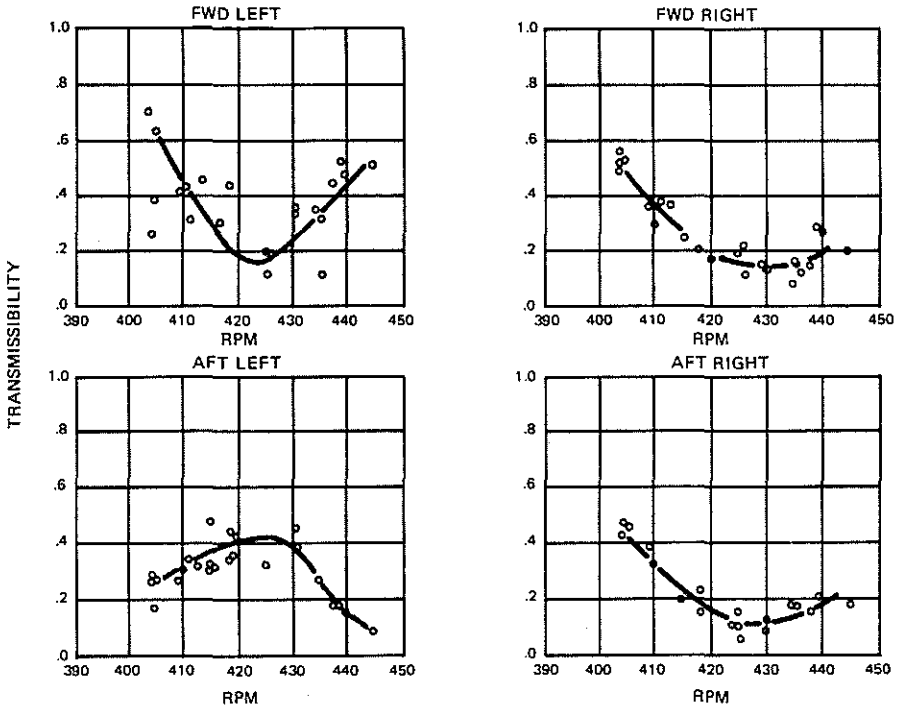

Figure 22. BO-105 In-Flight. 8/REV Transmissibility with Multi Frequency Isolator

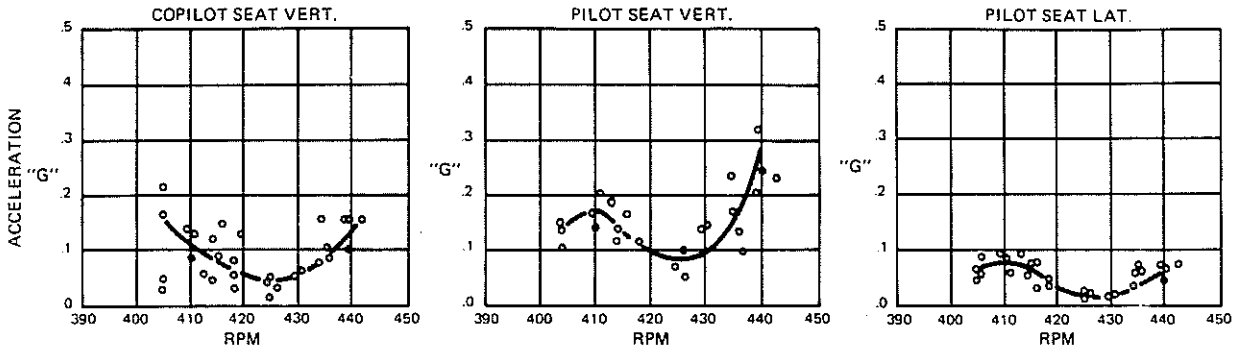

Figure 23. Partial Power Descent 8/REV Vibration in Cockpit with Multi Frequency Isolator

Application of Rotor Isolation to the YUH-61A

Initially, a program was carried out with Kaman to design elastomeric spring units for the YUH-61A (Figure 24) in parallel with the BO-105 units shown previously Figure 8. Similarly, shake testing of the YUH-61A units showed that these units were not sufficiently effective to provide the low vibration levels required. Subsequent data analysis showed that the damping was too high for effective isolation.

The analytical and test program of the BO-105 system with metal springs provided a basis for the detail design of the YUH-61A IRIS, which was initiated in December 1975.

A 24-degree-of-freedom analytical model was used to understand the natural frequencies and forced response of the rotor-isolation system for the YUH-61A. With this analysis the vertical and lateral spring rates and isolator characteristics were defined. The combination selected of 45,000 lb/in. vertical and 4,000 lb/in. lateral ensured that the natural frequencies introduced by the rotor-isolation system would be located between 1 and 4/REV and avoid the integer-frequency ratios. The effect of lateral stiffness on these frequencies is seen in Figure 25; the selected 4,000 lb/in. lateral stiffness ensures that the two mainly-roll frequencies are well below 4/REV.

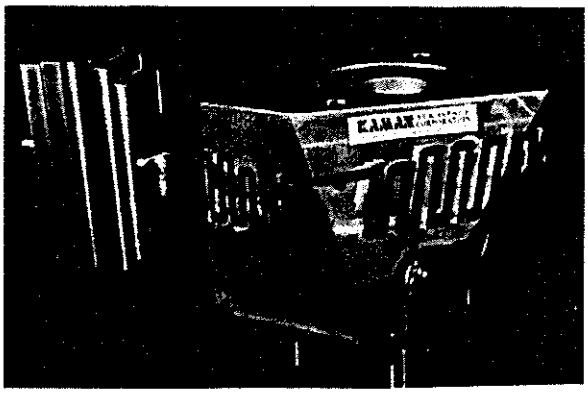

Figure 24. YUH-61A Elastomeric Isolator Unit

Subsequent BO-105 flight data has confirmed that roll excitation is the predominant cause of 4/REV airframe response in the regions of high vibration. Analysis of the forced response for rotor-roll excitation with and without the isolators shows the reductions at 4/REV and the increased response (only if excited) at lower frequencies.

In Figure 26, the vertical acceleration at the pilot's seat is shown resulting from rotor roll excitation, using the 24-degree-of-freedom forced-response analysis with and without the rotor-isolation system in operation. Some natural frequencies which cause resonant amplification are associated with blade natural frequencies and are present with or without isolation. Other

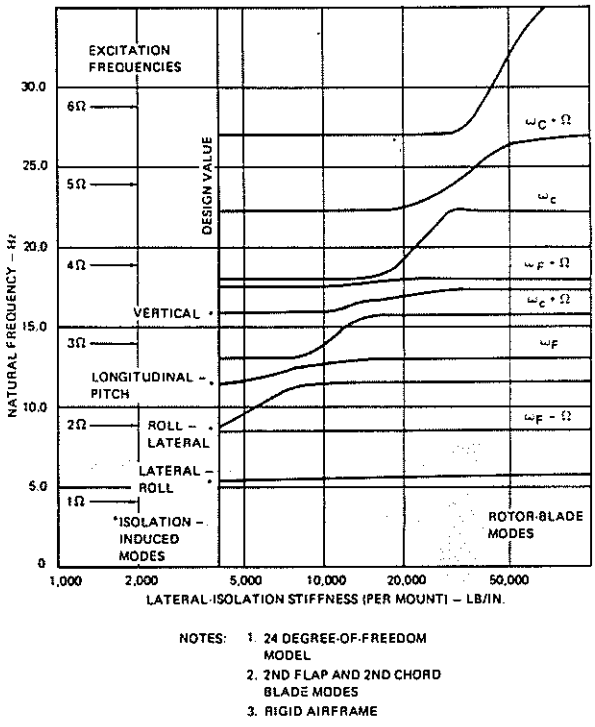

Figure 25. Effect of Lateral Isolation Stiffness on Rotor/Airframe Natural Frequencies

natural frequencies are only introduced by the isolation. The figure shows the reduction in vertical and lateral vibration caused by the isolation; it also shows that the frequencies introduced by the isolation will not result in resonant response due to residual excitations at 1, 2, or 3/REV.

Spectral analysis of isolated BO-105 flight data, which has similar natural frequencies introduced by the isolation, shows no change in response at integer-frequency ratios other than 4/REV (Figure 28).

The company-owned UTTAS design is based on metal springs for each of the vertical-isolator units. As shown in Figure 27 each spring is a steel torsion bar and the transmission leg is attached to the unit by a clevis through a gimbal arrangement to accommodate small angular motions of the transmission in pitch and roll. The anti-resonant bar of the vertical isolator is pivoted to the airframe and transmission by bearings. The transmission pivot connects to the transmission leg by a flexural rod allowing for the lateral motions, the shortening effect of bar angular motion, and the pitch and roll motions of the transmission. Lateral flexibility was provided in the YUH-61A by means of a laminated elastomeric bearing on the lateral-gimbal axis. The stiffness of this bearing is 4,000 lb/in. per leg; i.e., less than 1/10 of the vertical-isolator stiffness of 45,000 lb/in. This arrangement resulted in a compact unit suitable for the existing YUH-61A configuration and was installed with minimal airframe modifications. (Fig. 30)

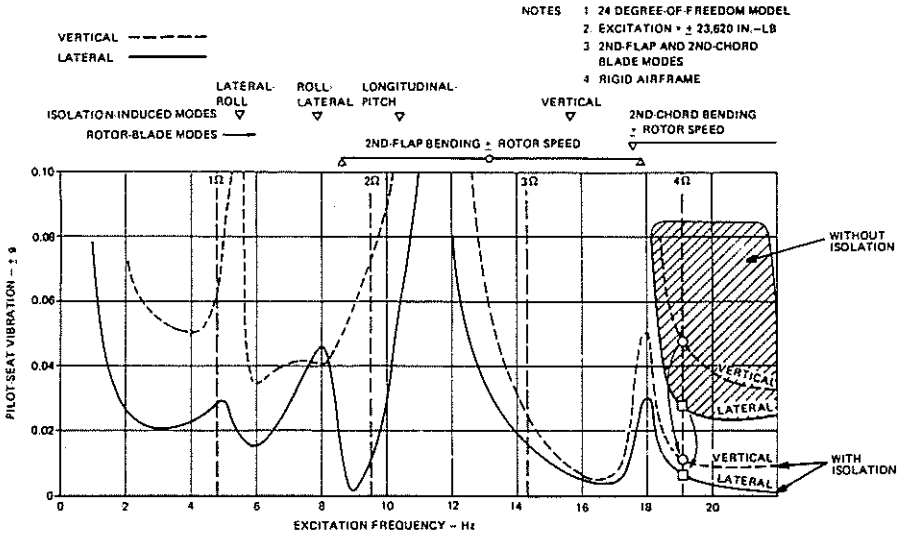

Figure 26. Response of Pilot's Seat to Rotor Excitation With and Without Rotor Isolation

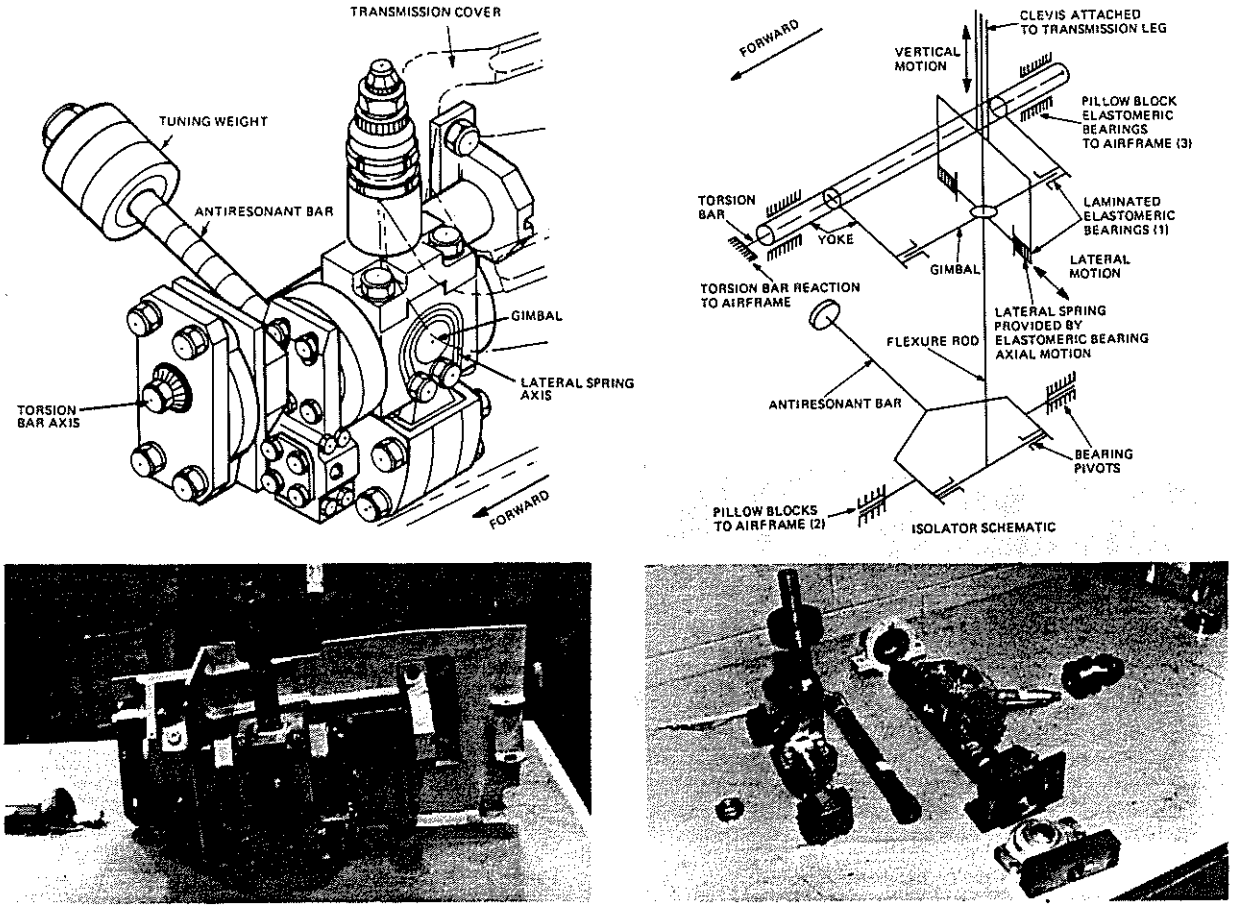

Figure 27. Typical Vertical Isolator for the YUH-61A

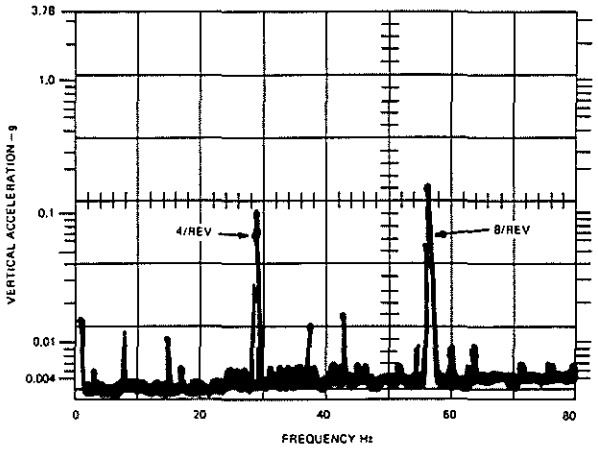

Figure 28. Spectral Analysis of BO-105 Cockpit Vertical Vibration in Partial-Power Descent with Isolation

The lateral antiresonant bar shown in Figure 29. is aligned longitudinally under the transmission. The bar reacts to the airframe by an axial member as in the BO-105 design.

The vertical travel of the vertical-isolator units is designed to allow 0-2g maneuvers at alternate gross weight, full cg range, without bottoming.

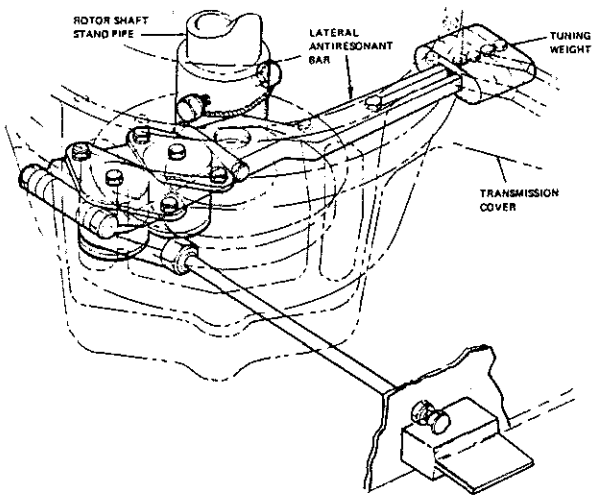

Figure 29. Typical Lateral Isolator for the YUH-61A

Bench tuning of the YUH-61A vertical isolators was performed in April, 1976 on a rig incorporating improvements derived from tuning the BO-105 units. One isolator is suspended between masses of 2500 and 700 pounds as shown in Figure 31. These masses represent ¼ of the dynamically equivalent masses of the airframe and rotor, respectively. Shaking is applied from below (representing rotor shaking) and additional steady loads are applied, representing rotor torque via low-spring-rate packs, to allow tuning under maneuver loads in the range of 0-2g.

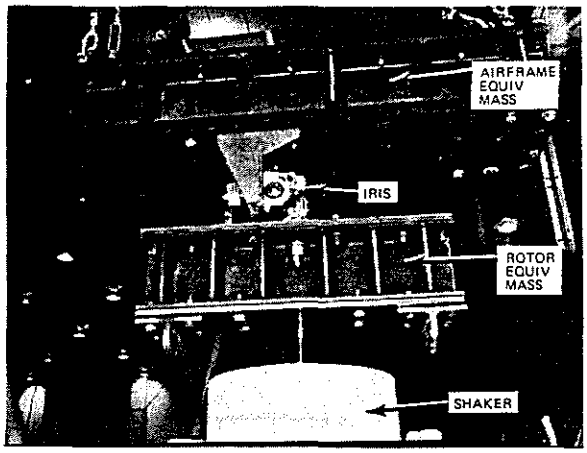

Figure 31. YUH-61 Isolator Tuning Rig

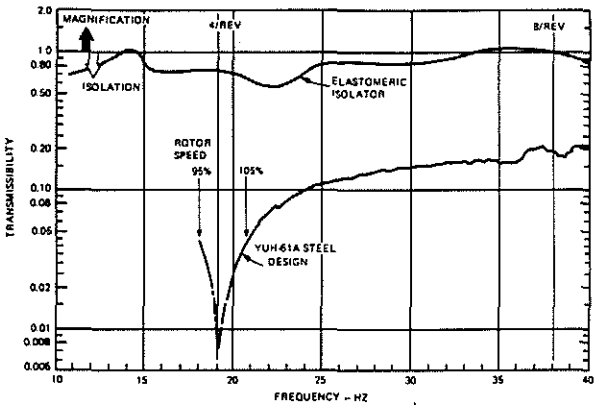

Figure 32. Transmissibility of the YUH-61A Isolation in Bench Test

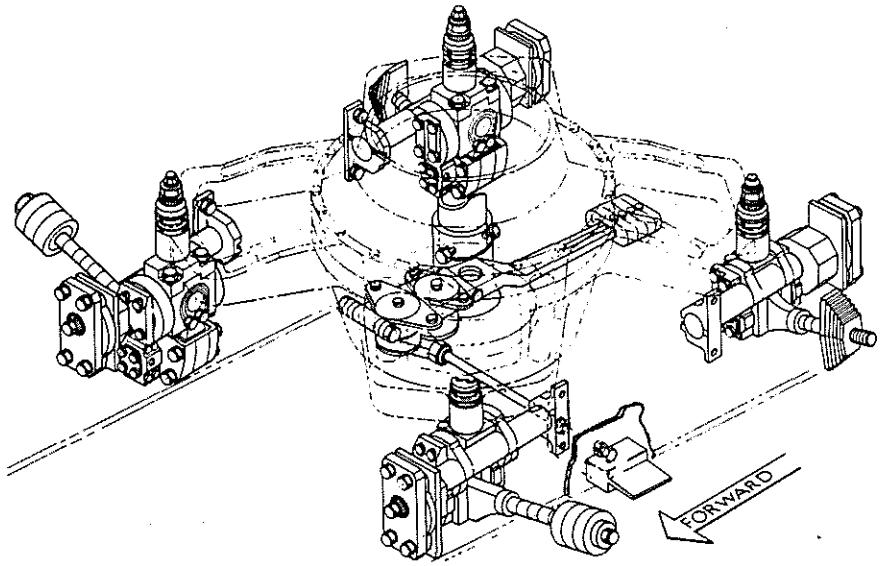

Figure 30. Arrangement of the YUH-61A Rotor-Isolation System

Isolation characteristics of the YUH-61A units, shown in Figure 32 are not only substantially better than the first elastomeric units because of the reduced damping but also have significantly improved on the successful BO-105 units by showing improved transmissibility (0.007) compared to 0.035), as well as reduced transmissibility at 8/REV (0.2 compared to 1.05).

At the time of writing for this paper for Company-owned YUH-61A has made its first flight with the IRIS installed. Confirming the bench testing, vibration accelerometer data recorded above and below the isolator units have shown transmissibility (Figure 33) even lower than achieved on the BO-105 IRIS. A rotor speed sweep conducted at 150 knots in level flight shows transmissibility similar to bench test data indicating 96-99% isolation at normal rotor speed. The resulting vibration transmitted to the airframe averages 0.05g (Fig. 34) and has provided an encouraging start to the further development of the system.

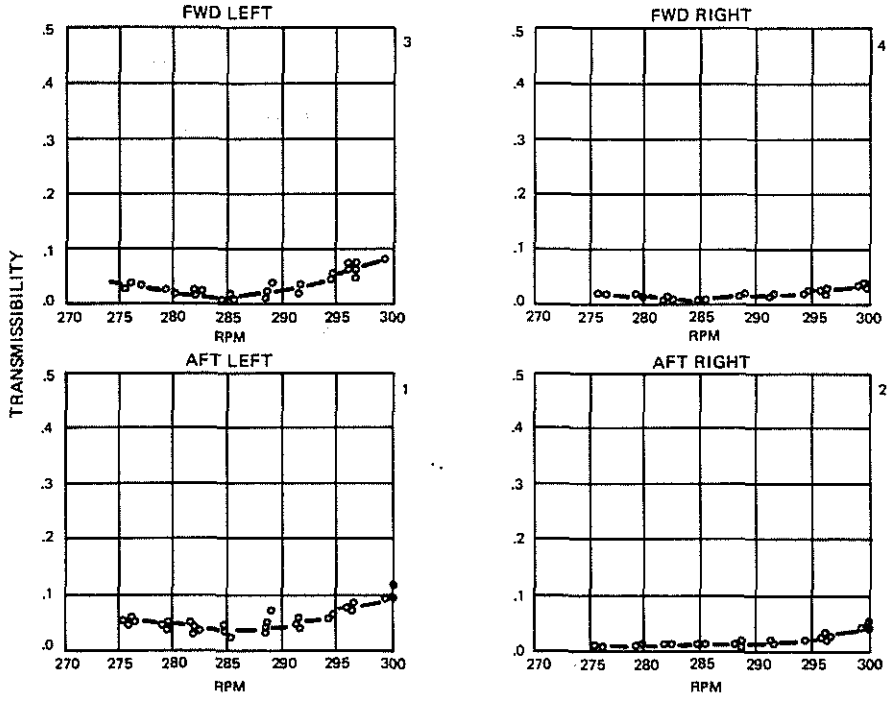

Figure 33. YUH-61A IRIS Transmissibility at 150 Kts

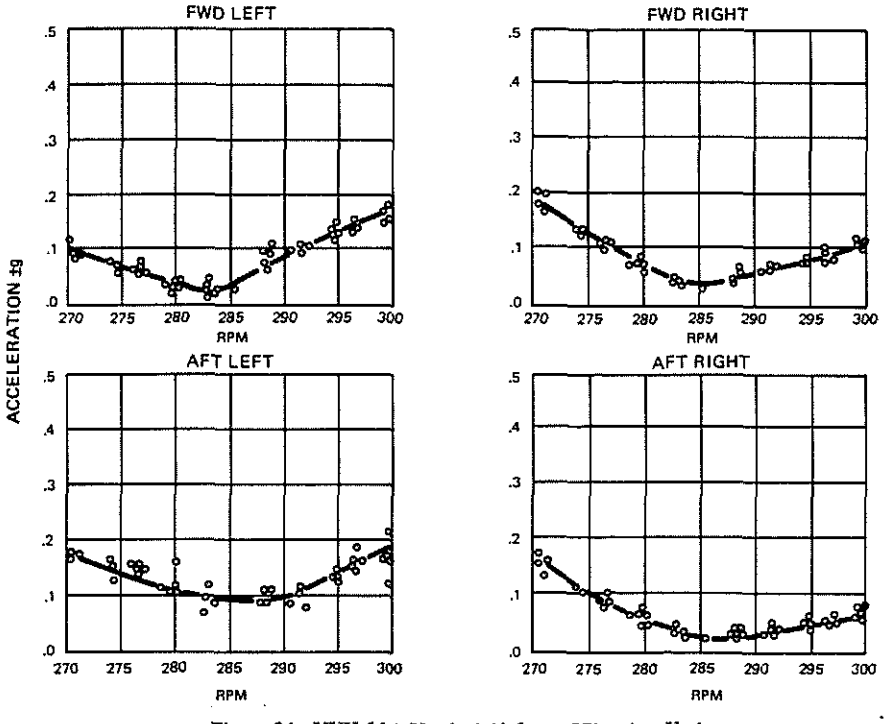

Figure 34. YUH-61A Vertical Airframe Vibration Under Isolators at 150 Kts

Complete design of a production system for the UH-61 shows that the weight penalty will be less than 1.5% gross weight. This is achieved by combining the spring assembly and the bar assembly into a single unit and eliminating many of the bearings which were part of the prototype assembly.

Conclusion

The BO-105 and YUH-61 programs have demonstrated that rotor isolation of the 4-bladed hingeless rotor is successful and practical. The key of this success has been a multi-axis arrangement system using low damping metal isolators. Dramatic vibration reduction has been achieved with no impairment of the agility and handling qualities.

References

1. A. Vecca, *"Vibration Effects on Helicopter Reliability and Maintainability."* USAAMRDL Technical Report 73-11, 1973.

2. D. L. Kidd, R. W. Balke, W. F. Wilson, and R. K. Wernicke, *"Recent Advances in Helicopter Vibration Control."* Paper presented at 26th Annual AHS National Forum, Washington, June 1970.

3. J. J. O'Leary, *"Reduction in Vibration of the CH-47C Helicopter using Self-tuning Vibration Absorbers,"* presented at Shock and Vibration Symposium, December 1969.

4. Amer, K. B. and Neff, J.R., *"Vertical-Plane Pendulum Absorbers for Minimizing Helicopter Vibratory Loads."* American Helicopter Society and NASA/Ames Research Center Specialists Meeting on Rotorcraft Dynamics, Moffett Field, Calif., Feb. 1974, NASA SP-352.

5. R. B. Taylor, P. A. Teare, *"Helicopter Vibration Reduction with Pendulum Absorbers,"* Paper presented at 30th annual AHS National Forum, Washington, June 1970.

6. Von Hardenberg, P. W. and Sattanis, P. B., *"Preliminary Development of an Active Transmission Isolation System,"* 27th Annual AHS National Forum, Washington, May 1971.

7. Calcaterra, P. C. and Schubert, D. W., *"Isolation of Helicopter Rotor-Induced Vibrations Using Active Elements,"* USAAVLABS Technical Report 69-8, U.S. Army Aviation Materiel Laboratories, Ft. Eustis, Virginia, June 1969.

8. Kidd, D. L., Balke, R. W., Wilson, W F., and Wernicke, R. K., *"Recent Advances in Helicopter Vibration Control,"* 26th Annual AHS National Forum, Washington, June 1970.

9. Flannelly, W. G., *"The Dynamic Anti-Resonant Vibration Isolator,"* 22nd Annual AHS National Forum, Washington, May 1966.

10. A. D. Rita, J. H. McCarvey, R. Jones, *"Helicopter Rotor Isolation Evaluation Utilizing the Dynamic Antiresonant Vibration Isolator,"* 32nd Annual AHS National Forum, Washington, May 1976.

11. Shipman, D. P., White, J. A., and Cronkite, J. D., *"Fuselage Nodalization,"* 28th National Forum of the American Helicopter Society, Washington, D. C., May 1972.

Copies of this paper may be obtained by writing to the Boeing Vertol Company, Technical Library, P.O. Box 16858, Philadelphia, Pennsylvania 19142.